



**HAL**  
open science

## Spatial mechanistic modeling for prediction of the growth of asymptomatic meningioma

Annabelle Collin, Cédric Copol, Vivien Pianet, Thierry Colin, Julien Engelhardt, Guy Kantor, Hugues Loiseau, Olivier Saut, Benjamin Taton

► **To cite this version:**

Annabelle Collin, Cédric Copol, Vivien Pianet, Thierry Colin, Julien Engelhardt, et al.. Spatial mechanistic modeling for prediction of the growth of asymptomatic meningioma. *Computer Methods and Programs in Biomedicine*, In press. hal-02397720v3

**HAL Id: hal-02397720**

**<https://inria.hal.science/hal-02397720v3>**

Submitted on 19 Dec 2019 (v3), last revised 15 Dec 2020 (v4)

**HAL** is a multi-disciplinary open access archive for the deposit and dissemination of scientific research documents, whether they are published or not. The documents may come from teaching and research institutions in France or abroad, or from public or private research centers.

L'archive ouverte pluridisciplinaire **HAL**, est destinée au dépôt et à la diffusion de documents scientifiques de niveau recherche, publiés ou non, émanant des établissements d'enseignement et de recherche français ou étrangers, des laboratoires publics ou privés.

# Spatial mechanistic modeling for prediction of the growth of asymptomatic meningiomas.

Annabelle Collin<sup>1</sup><sup>\*</sup>, Cédric Copol<sup>1</sup>, Vivien Pianet<sup>2</sup>, Thierry Colin<sup>2</sup>, Julien Engelhardt<sup>3</sup>, Guy Kantor<sup>4</sup>, Hugues Loiseau<sup>3,5</sup>, Olivier Saut<sup>1</sup>, Benjamin Taton<sup>1,6</sup>

**1** Univ. Bordeaux, Inria Bordeaux-Sud-Ouest, Bordeaux INP, CNRS, IMB, UMR 5251, F-33400, Talence, France

**2** Sophia Genetics, Cité de la Photonique, F-33600, Pessac, France

**3** Service de Neurochirurgie B, Groupe Hospitalier Pellegrin, CHU Bordeaux, F-33000, Bordeaux, France

**4** Département de Radiothérapie, Institut Bergonié, F-33076 Bordeaux, France

**5** EA 7435 - IMOTION, Univ. Bordeaux, F-33076, Bordeaux, France

**6** Service de Néphrologie - Transplantation - Dialyse - Aphérèses, Groupe Hospitalier Pellegrin, CHU Bordeaux, F-33000, Bordeaux, France

 These authors contributed equally to this work.

## Abstract

Mathematical modeling of tumor growth draws interest from the medical community as they have the potential to improve patients' care and the use of public health resources. The main objectives of this work are to model the growth of meningiomas – slow-growing benign tumors requiring extended imaging follow-up – and to predict tumor volume and shape at a later desired time using only two time examinations. We propose two variants of a 3D partial differential system of equations (PDE) which yield after a spatial integration systems of ordinary differential equations (ODE) that relate tumor volume with time. Estimation of models parameters is a crucial step for obtaining a personalized model for a patient that can be used for descriptive or predictive purposes. As PDE and ODE systems share the same parameters, they are both estimated by fitting the ODE systems to the tumor volumes obtained from MRI examinations acquired at different times. A population approach allows to compensate for sparse sampling times and measurement uncertainties by constraining the variability of the parameters in the population. Description capabilities of the models are investigated in 40 patients with benign asymptomatic meningiomas who had had at least 3 surveillance MRI examinations. The two models can fit to the data accurately and more realistically than a naive linear regression. Prediction performances are validated for 33 patients using a population approach. Mean relative errors in volume predictions are less than 10% with ODE systems versus 12.5% with the naive linear model using only two time examinations. Concerning the shape, the mean Sørensen-Dice coefficients are 85% with the PDE systems in a subset of 10 representative patients.

## Introduction

Mathematical modeling of tumor growth has recently drawn interest from the medical community. Indeed, since the pioneering work on glioblastomas [1], the development of such reliable models has helped better understand biological mechanisms and clinical behaviors of several types of tumor such as lung metastases [2], renal cell carcinoma [3], and glioblastoma [1, 4] or the effects of treatments [5–7]. Such applications are made possible mainly thanks to the development of realistic mathematical models which are personalized using patients’ imaging.

In this work, we have set our sights on intracranial meningiomas. Arising from arachnoidal cap cells, they account for a third of primary adult intracranial tumors [8,9]. They become a major public health issue: (1) an annual increasing incidence ranging from 2-4.5% has been reported [8–10] and (2) one third of these tumors are asymptomatic at the time of diagnosis [8–12]. While most meningiomas are slow-growing tumors (about 80% are classified grade I, namely benign meningioma), some may exhibit important growth over a short period of time. Recent data have shown that asymptomatic meningiomas are observed in 1% to 2% of the population, especially in women over 60 years of age [13–15]. Surgery or radiation therapy remain the cornerstone of the treatment for meningiomas, and, following the diagnosis of asymptomatic lesions, clinicians struggle with the decision of either immediately treating the lesion using these invasive procedures, or simply planning periodical radiological examinations [16–22]. In most cases, the frequency of such a monitoring is based on empirical strategies [11, 20–30]. This is not optimal due to the potential toxicity of repeated Gadolinium infusions [31] and from a medico-economic point of view. Consequently, predicting the progression of asymptomatic lesions is paramount to inform decision-making. However, to our knowledge, only one predictive tool [32–34] is available to assess the growth rate of untreated meningiomas and help clinicians in selecting which patients to treat or simply monitor. This tool was developed based on statistical predictions (logistic regression) using various clinical and imaging findings collected at the time of diagnosis as covariates. In this context, mathematical modeling of the underlying physiopathological processes can offer an accurate alternative in terms of prediction of growth.

In this work, using a mathematical models of meningiomas growth, we show that patient-specific growth parameters can be recovered from two of successive MRI examinations. Numerical simulations of the disease evolution may then be used to predict the volume and the shape of the tumor at a later time, an information that could prove valuable to inform medical decisions, adapt follow-up and hence optimize the use of public health resources.

The outline of the paper is as follows. In Section 1, the patients cohort and the associated data are presented. In Section 2 different models are presented. We consider spatio-temporal evolution of populations of tumor cells controlled by a “carrying capacity” parameter. In this work, spatially distributed and spatially independent carrying capacities will be confronted then two models will be derived. These two models have the form of partial differential equation (PDE) systems. They can be reduced to ordinary differential equation (ODE) systems that will be used to adapt the model to each patient by estimating the parameters. In Section 3, a validation of ODE and PDE models is done using the full cohort with all the available times. The objective of this section

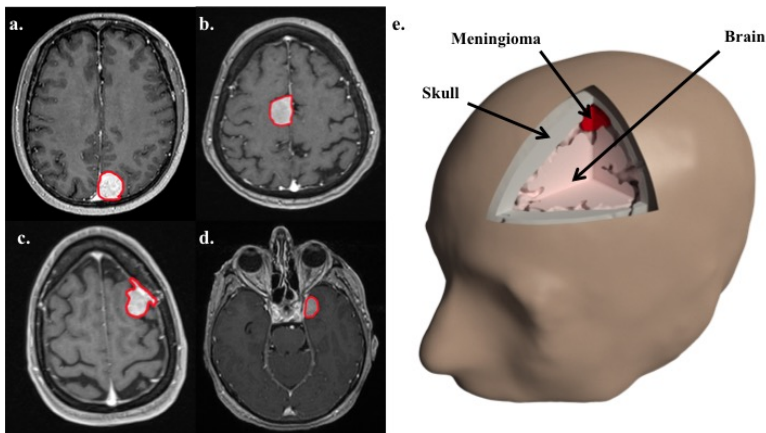


**Fig 1. Examples of meningioma geometry (a,b,c,d) from MRI T1 sequences with gadolinium-based contrast media. Tumor boundaries are highlighted in red. (e) Anatomical view of a meningioma: 3D reconstruction with a homemade segmentation tool from the medical images. The head, skull, brain and meningioma geometries are delineated in 3D from the MRI examination.**

is to assess the descriptive power in terms of tumor volume and shape of our models. Finally, in Section 4, we will assess the predictive power (also in terms of tumor volume and shape) of our models in order to see if using only two MRI examinations, we can predict the volume and the shape of the tumor, at a later time.

## 1 Available data and objectives

A monocentric prospective cohort of patients diagnosed with asymptomatic meningioma has been studied. Patients were included in the study if at least 3 gadolinium-enhanced T1-weighted MRI (acquired on various devices) were available. Patients for which the technical quality of the available MRI acquisitions was too low were excluded (*e.g.* too large thickness of the slices). The study and the use of the MRI images were approved by our institutional review board. Inform consents for data collection were waived for research for all patients, in accordance with the related policy of Bordeaux University Hospital.

Clinical information (age, gender and meningioma position) of the cohort and times and volumes of available MRI examinations are given in Table 1. The cohort is composed of 40 patients with between 3 and 6 MRI acquired during follow-up. We have excluded Patient 24 because it was not possible to properly quantify the evolution of his meningioma, due to poor quality of his MRI examinations.

The lesion, as well as the skull are segmented using homemade software developed by B. Taton that relies on a deformable model in the principle of [35]. Illustrations of the segmentation process are given in Fig 1. Using this tool, we have extracted for each patient of the cohort the volumes and the shapes of the tumor at each time.

Using these data, we want to answer two questions:

Pat.	Age	G	Pos.	Times [months]	Volumes [cm <sup>3</sup> ]
1	52	F	ER	0   5   13   25	0.7   0.8   0.9   1.7
2	48	M	BLPS	0   6   14	6.1   6.3   6.4
3	50	F	BRPM	0   31   67   93	2.2   3.5   3.7   4.0
4	53	F	BMPS	0   5   21   44	4.4   4.7   5.6   7.7
5	33	F	BLPI	0   20   32   50	1.5   2.7   3.6   5.7
6	44	F	IMAM	0   28   40   52	1.7   2.3   2.7   3.2
7	34	F	BLAS	0   12   24	1.2   1.9   2.7
8	70	F	ELI	0   5   10	1.0   2.0   3.4
9	77	F	BLPI	0   23   42	0.6   1.5   3.3
10	50	F	IRAS	0   39   62   95	13.4   15.5   15.9   16.3
11	52	M	BRAS	0   32   62	1.3   1.7   1.8
12	60	F	BRAS	0   74   86	4.9   7.6   7.7
13	64	F	ER	0   6   12   29   53	2.3   2.5   2.9   3.6   4.2
14	34	F	EL	0   11   37   61   68   81	2.8   3.0   4.0   6.0   6.2   6.8
15	57	F	BRMI	0   38   83	1.5   2.2   2.6
16	39	F	BMAS	0   7   14   22   34	1.0   1.7   2.1   2.0   2.2
17	66	F	BRMS	0   13   33   59	4.2   4.0   4.0   4.4
18	52	F	BLMS	0   7   21	3.5   4.9   6.9
19	62	F	ER	0   30   46   60	2.5   3.1   3.6   3.9
20	53	F	BRPM	0   7   21	0.6   0.8   0.8
21	69	F	IMMS	0   6   23   39	10.4   10.4   12.2   13.1
22	80	F	ELI	0   8   10	2.5   5.6   7.1
23	45	M	IMAS	0   7   15	5.5   5.7   6.3
25	49	F	EM	0   7   14   26	2.6   3.1   3.6   3.5
26	46	F	BRAS	0   6   21   37	1.9   1.9   2.1   2.3
27	58	F	ER	0   6   13   40	2.5   2.5   2.6   2.7
28	81	F	BMPI	0   20   43   64	1.9   3.3   5.8   7.6
29	40	F	ER	0   5   13   33	0.4   0.4   0.5   0.8
30	40	F	ER	0   5   13   33	0.1   0.1   0.2   1.2
31	44	F	IMPS	0   4   7   33	0.5   0.6   0.6   0.8
32	69	F	BLAS	0   7   14	1.6   1.7   2.0
33	39	F	EL	0   7   23	1.7   1.9   1.9
34	39	F	EL	0   7   23	2.8   2.7   3.1
35	64	F	BLAS	0   27   46	5.6   5.8   6.1
36	47	F	EL	0   6   12	1.2   1.2   1.9
37	66	F	ER	0   5   12	0.9   0.9   1.1
38	52	F	BMPS	0   5   13	1.8   1.7   2.1
39	79	F	IMMS	0   10   25	1.3   1.3   1.6
40	48	F	BMPM	0   18   29	2.1   3.0   3.9

**Table 1. Presentation of the patient cohort: age at diagnostic, gender, meningioma position, times and volumes of available examinations.**

The position is summarized by 2 or 4 letters where letters indicate at the first position, B border, I interior, E eye, and at the other positions: L left, R right, A anterior, P posterior, I inferior, S superior and M middle.

- Can we model the dynamics of meningioma evolution?
- Using only two MRI examinations, can we predict the volume and the shape of the tumor, at a later time?

To answer the first question, we build two 3D mechanical models of tumor growth. These models depend on parameters which have to be estimated for each patient. As these models can be reduced to ODE systems corresponding to the volume evolution with respect to time and depending on the same parameters as the PDE systems, the estimation process can be performed on these OD equations. To validate the models, the full cohort with all the available times will be used to fit the ODE systems to the data and then assess their descriptive power.

To answer the second question, we use only the 2 first available MRI examinations to estimate the parameters of the models and then predict the volume and the shape of the tumor at a later time corresponding to the time of the third available examination. This allows us to evaluate the predictive power of our models.

## 2 Modeling of meningiomas evolution

In this section, we describe the spatio-temporal evolution of populations of tumor cells that is controlled by a “carrying capacity” parameter (in the spirit of [36]). In this work, spatially distributed and spatially independent carrying capacities are investigated hence deriving two different models. These two models are based on systems of partial differential equation (PDE) as shown in Section 2.1. These systems can be reduced to ordinary differential equation (ODE) systems, see Section 2.2, that are used to parametrize the model.

### 2.1 Spatial model, PDE system

Let  $\mathcal{B}$  be a bounded and smooth domain of  $\mathbb{R}^3$ . The evolution of the density  $T$  of proliferative cells is supposed to satisfy the following equation:

$$\partial_t T + \nabla \cdot (\vec{v}T) = MT, \quad \mathcal{B} \quad (1)$$

where  $\vec{v}$  denotes the velocity field that describes the motion of tumor cells. The growth rate is denoted by  $M(t, X)$ . In this work, two different dynamics of the growth rate are considered:

$$M = M_0 e^{-\alpha t} \text{ (equivalent to } \partial_t M = -\alpha M)$$

and

$$\partial_t M = -\alpha MT$$

where in both cases  $\alpha^{-1}$  corresponds to the characteristic time at which the tumor growth capacity decreases and  $M_0$  is a constant corresponding to the initial growth rate. In the first case, the growth rate only depends on  $t$  - which could be seen as an oversimplifying assumption -, in the second case it also depends on the space variable  $X$ .

We denote by  $S(t, X) = 1 - T(t, X)$  the density of healthy tissue and we assume that  $S(t, X)$  is only advected at the velocity  $\vec{v}$  due to cellular division of

cancer cells. This is clearly not true (for example, there is a biological action of the tumor on the extracellular matrix), but in our setting, this assumption means that the global evolution of the tumor is not modified by the extra-tumoral medium. This reads

$$\partial_t S + \nabla \cdot (\vec{v}S) = 0, \quad \mathcal{B}. \quad (2)$$

Using  $T + S = 1$  (it is a saturation hypothesis) leads to (using Eq (1))

$$\nabla \cdot \vec{v} = MT, \quad \mathcal{B}. \quad (3)$$

Eq (3) is clearly not enough to close the system and we assume in addition the following Darcy's law

$$\vec{v} = -\nabla\pi, \quad \mathcal{B}, \quad (4)$$

where  $\pi$  is the pressure. Eqs (3) and (4) lead to

$$-\Delta\pi = MT, \quad \mathcal{B}. \quad (5)$$

Eq (5) is solved in  $\mathcal{B}$  that is the intersection of the inside of the skull with a cube centered on the tumor. The boundary of the cube is denoted by  $\Gamma = \partial\mathcal{B}$ . The part of the skull that is included in the cube is denoted by  $\Gamma_1$ . The boundary condition on  $\Gamma_1$  is

$$\frac{\partial\pi}{\partial n} = 0 \quad (6)$$

and is implemented by a penalty method. On  $\Gamma \setminus \Gamma_1$  we impose

$$\pi = 0. \quad (7)$$

The domain  $\mathcal{B}$  is taken large enough such that (7) has no significant influence on the growth. Mechanically speaking, Eqs (4) and (5) imply that the increase of volume due to the tumor growth generates locally an increase of pressure. The pressure gradient creates a movement at velocity  $\vec{v}$  in its opposite direction. Developing Eq. (1) yields

$$\partial_t T + \vec{v} \cdot \nabla T = MT(1 - T). \quad (8)$$

Let the initial condition of  $T$  equal to  $T(0, x) = 1$  inside the tumor and 0 elsewhere, one can easily see that  $T(t, X) = 1$  inside the tumor and 0 elsewhere at any time. We define by  $\Omega(t) = \{x, T(t, x) > 0\}$  the domain corresponding to the tumor at time  $t$ .

To conclude this section, it is clear than one could probably write a model for tumor growth closer to biology but the major advantage of these two models is that they depend only on two parameters:  $M_0$  and  $\alpha$ . We choose to keep the models simple to ensure that they can effectively be personalized for each patient using the sparse observations that are available in the clinical routine.

## 2.2 An ODE system embedded in the PDE system

Let us denote by  $V(t)$  the volume of the lesion  $\Omega(t)$  at time  $t$ . We have

$$V(t) = \int_{\mathcal{B}} T(t, X) dX = \int_{\Omega(t)} dX$$

by definition of  $T$ . One can prove the two following propositions (see Appendix for the proofs).

	Time-d. $M_0$	Space/time-d. $M_0$	Linear mod.
$\mathcal{E}_d$	1.7%	1.5%	5.2%

**Table 2. Descriptive power - Relative error  $\mathcal{E}_d$  (see Eq. (12))**

**Proposition 1** *If  $M = M_0 e^{-\alpha t}$ , we have:*

$$V(t) = V_0 e^{\frac{M_0}{\alpha}(1-e^{-\alpha t})}. \quad (9)$$

**Proposition 2** *If  $\partial_t M = -\alpha M T$ , we have:*

$$V(t) = V_0 + M_0 V_0 \frac{e^{(M_0-\alpha)t} - 1}{M_0 - \alpha}. \quad (10)$$

For the estimation process, we define  $\beta = M_0 - \alpha$ . Let us note that the volume evolution  $V$  is linear if and only if  $M_0 = \alpha$  and in this case

$$V(t) = V_0 + V_0 M_0 t. \quad (11)$$

As we have  $\frac{e^{(M_0-\alpha)t}-1}{M_0-\alpha} > 1$  (resp.  $\frac{e^{(M_0-\alpha)t}-1}{M_0-\alpha} < 1$ ) if  $M_0 > \alpha$  (resp.  $M_0 < \alpha$ ), three behaviors for  $V$  are possible:

- $M_0 = \alpha$ :  $V$  is linear,
- $M_0 > \alpha$ :  $V$  is exponential (strictly convex),
- $M_0 < \alpha$ :  $V$  is strictly concave.

For the parametrization process, instead of estimating  $\alpha$ , we will estimate  $\beta = M_0 - \alpha$  using as *a-priori*  $\beta = 0$ .

### 3 Evaluation of the descriptive power of the models

To validate the models, the full cohort with all the available times is used to fit the ODE systems to the data and then assess their descriptive power. We start by investigating the prediction of the tumor volume then its shape.

#### 3.1 Tumor volume

To estimate the two constant parameters  $\alpha$  (resp.  $\beta$ ) and  $M_0$  of the 0D model (9) (resp. (10)), a population approach has been chosen. The mixed-effect approach [37] consists of pooling all the patients together and estimating a global distribution of the model parameters in the population. More precisely, the individual parameters  $\alpha^j$ ,  $\beta^j$  and  $M_0^j$  (where  $j$  denotes the individual) are assumed to be realizations of a random variable decomposed into two parts:

$$\begin{aligned} \{\alpha, \beta\}^j &= \{\alpha, \beta\}^{pop} + \{\tilde{\alpha}, \tilde{\beta}\}^j, \forall j \in [1, N_p], \\ M_0^j &= M_0^{pop} + \tilde{M}_0^j, \forall j \in [1, N_p], \end{aligned}$$

where  $N_p$  is the number of considered patients,  $\alpha^{pop}$ ,  $\beta^{pop}$  and  $M_0^{pop}$  correspond to the fixed effects where as  $\tilde{\alpha}^j$ ,  $\tilde{\beta}^j$  and  $\tilde{M}_0^j$  correspond to the random effects and

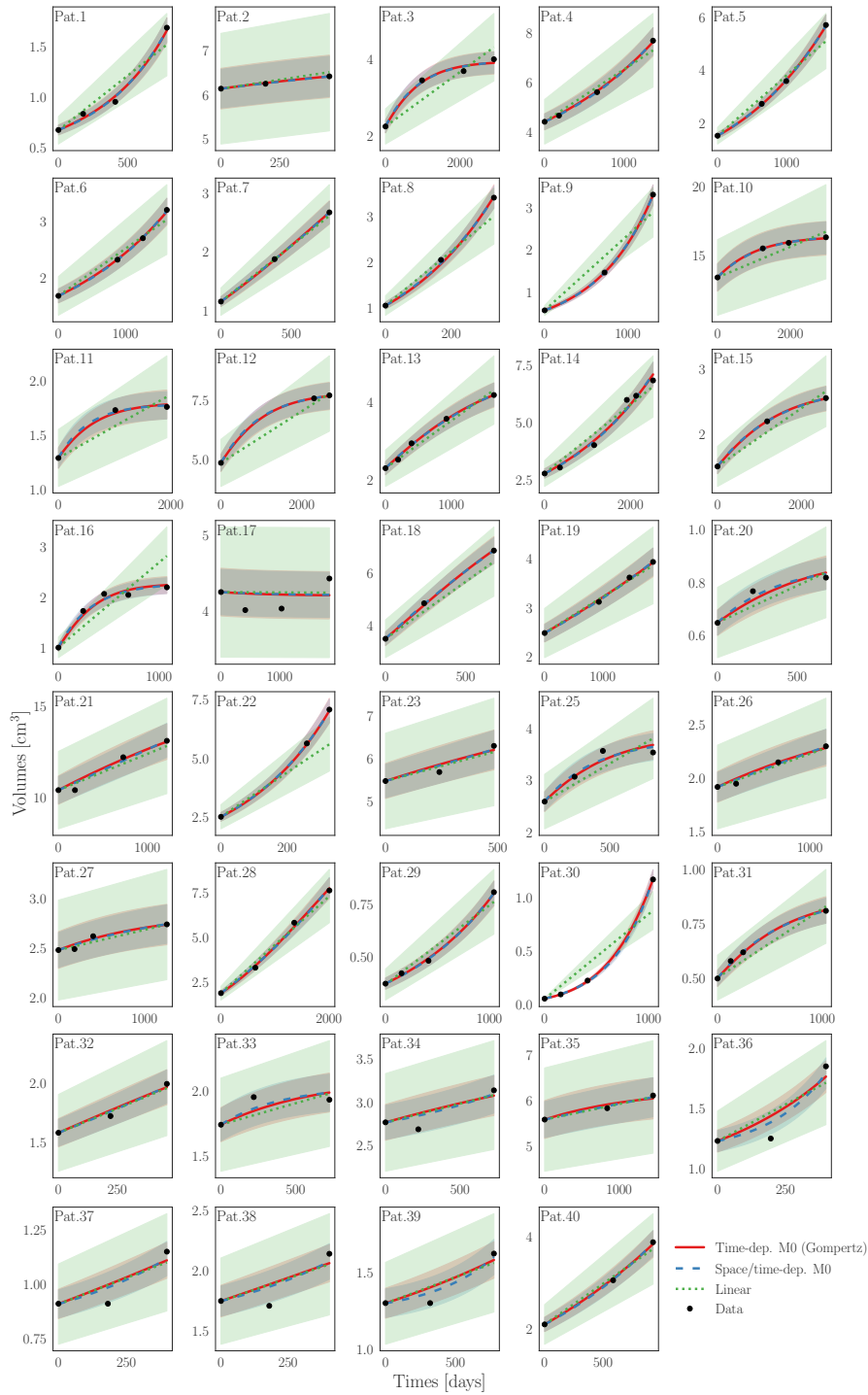


**Fig 2. Descriptive power - Estimated volumes compared to the data for the full cohort. The tumor volumes obtained using MRI segmentations are represented by black circles. The red (resp. blue and green) curves correspond to the model with time-dependent growth rate (9) (resp. to the model with space- and time-dependent growth rate (10) and to the linear model (11)).**

have been assumed with mean zero. The parameters that we want to estimate are not physiological, there are no priors for their means and standard deviations. We then assume that

$$\alpha^{pop}, \beta^{pop} \sim \mathcal{N}(0, 0.01^2) \text{ and } M_0^{pop} \sim \mathcal{N}(0, 0.01^2),$$

emphasizing that these assumptions do not seem too restrictive.

Models (9) (time-dependent  $M_0$ ) and (10) (space- and time-dependent  $M_0$ ) also depend on the initial volume  $V_0$ . This value can be fixed with the volume computed using the first MRI examination but doing that does not allow to consider the uncertainty of the segmentation process. That is why we consider  $V_0^j$  of each patient  $j \in [1, N_p]$  as a covariate of the estimated volume at the initial time:

$$V_0^j = V_0^{j,MRI} + e_0^j,$$

where  $e_0^j \sim \mathcal{N}(0, 0.1^2)$ .

We assume that the measurement error for all volumes is proportional

$$V^{j,MRI}(t) = V^{j,estim}(t)(1 + e),$$

where  $V_k^{j,estim}$  corresponds to the estimated volume using ODE systems and  $e$  the measurement error. We assume that it follows a Gaussian law  $\mathcal{N}(0, 0.05^2)$ . The standard deviation of 5% is not arbitrary. It is the same order of magnitude found in [38] for lung or liver metastasis. This standard deviation is estimated  $\sigma_e$  and is used to define the 95% confidence interval:  $[V^{j,estim}(t)(1 - 1.96\sigma_e); V^{j,estim}(t)(1 + 1.96\sigma_e)]$ .

This estimation strategy is implemented in a software called Monolix [39], which maximizes the likelihood using the stochastic approximation expectation maximization (SAEM) algorithm [40]. For all the results obtained with Monolix in this paper, the convergence of the algorithm has been reached.

As the growth of meningioma is quite slow, a comparison with a linear model (for example Model (10) when  $\beta = 0$ ) will be done using the same hypothesis.

Fig 2 presents all the graphical representations of the results using the estimation process. Each figure gathers all the fits performed for a given patient: the tumor volumes obtained using MRI segmentations are represented by black circles. The red (resp. blue and green) curves correspond to the model with time-dependent growth rate (9) (resp. to the model with space- and time-dependent growth rate (10) and to the linear model (11)). The 95% confidence intervals are also represented as shaded areas. One can remark that the results obtained using the ODE models are similar. The following relative error is computed

$$\mathcal{E}_d = 100 \frac{1}{N_p} \sum_{p=1}^{N_p} \frac{1}{N_{p,e}} \sum_{e=1}^{N_{p,e}} \frac{|V(t_e) - V_e^{meas}|}{V_e^{meas}}, \quad (12)$$

for each model where  $N_{p,e}$  corresponds to the number of available examinations for each patient  $p$ ,  $V(t_e)$  to the estimated volume at time  $t_e$  corresponding to the  $e$ -th MRI examination,  $V_e^{meas}$  to the measurement volume at time  $t_e$ . Table 2 summarizes the results. One can note that the error  $\mathcal{E}_d$  is very small for the ODE models but also for the linear model. For the three models, errors are of the same order as the measurement error so that all these models are acceptable. However, one can see that the patients variability is not well represented using

Pat.	SDC (Time-d. $M_0$ )	SDC (Space/time-d. $M_0$ )
2	95%	95%
4	93%	93%
7	83%	83%
8	83%	86%
9	67%	67%
11	87%	87%
18	87%	86%
20	93%	93%
22	85%	85%
23	88%	88%

**Table 3. Descriptive power - Sørensen-Dice coefficient SDC (see Eq. (13)) as a comparison between the solution of the tumor growth model and the MRI segmentation at the last available time.**

the linear model. Indeed, the volume evolution when they are strictly convex, as for example for Patients 1, 5 and 9 (resp. concave, as for example for Patients 3, 10 and 11) are not well fitted using the simple linear model.

### 3.2 Tumor shape

As presented in Section 2, the meningioma growth in the skull can be simulated in 3D by the numerical resolution of two PDE systems (one with space- and time-dependent growth rate and one with time-dependent growth rate) leading after volume integration to the two ODE systems studied in the previous section.

The inputs of the simulation are the initial tumor cell density  $T(0, X)$  and the  $\alpha$  or  $\beta$  and  $M_0$  parameters determined by the parameterization of ODE systems (when  $V_0$  is fixed in order to have  $T(0, X)$  of volume  $V_0$ ). Simulation boundary conditions consist in the assumption that the meningioma growth is limited by the arachnoid tissue. The initialization  $T(0, X)$  and the boundary conditions are obtained via the segmentation of the second MRI examinations (see Fig 1).

The simulation is done using the following split-step scheme:

- Computes the potential  $\pi$  by solving the Poisson's equation (5) at time  $t$ .
- Estimates the cell transport velocity  $\vec{v}$  via the Darcy's law (4) and the velocity divergence  $\nabla \cdot \vec{v}$  (3) at time  $t + \Delta t$ .
- Computes the tumor cell density transport over the time step  $\Delta t$ .
- Computes the growth capacity  $M$  at time  $t + \Delta t$ .

The resolution of the tumor cell transport at each time is performed thanks to a second order splitting method with a fifth order WENO transport scheme. The simulation time step  $\Delta t$  used in the resolution is computed at each iteration to satisfy two conditions: (i) to be small enough to ensure the stability of the transport solution and (ii) not to exceed one day per simulation step.

The 3D simulation of the spatial growth of meningiomas has been performed in 10 cases – selected to represent the full cohort. The similarity between

	Time-d. $M_0$	Space/time-d. $M_0$	Linear mod.
$\mathcal{E}_p$	9.9 %	9.8%	12.5%
$\mathcal{B}_p$	0.007	-0.007	0.024

**Table 4. Predictive power - Relative error  $\mathcal{E}_p$  and bias  $\mathcal{B}_p$  at time  $t_2$  (see Eq. (14))**

simulations and registered MRI segmentations is measured with the Sørensen-Dice coefficient (SDC): given two sets, X and Y of discrete data, the SDC is defined by

$$\text{SDC} = \frac{2|X \cap Y|}{|X| + |Y|} \times 100, \quad (13)$$

where  $|X|$  and  $|Y|$  are the cardinalities of the two sets. We compare using this indicator the overlap between the spatial extension of the simulated tumor and the segmentation of the MRI data at the last available time.

Results are presented in Table 3. One can see that the shape of the tumor is very well estimated with a mean SDC of 86 % for both models. For Patients 2, 4 and 20, the very excellent results can be explained by the fact that the growth is very slow. Minimum (67 %) is obtained for Patient 9. This result is due to the fact that the shape of the tumor evolves in time (during the two first times  $t_0$  and  $t_1$ ). The two ODE systems presented in this work do not allow to consider time-evolving shapes: more complex models have to be used as presented in [41]. Results are satisfactory but do not permit to select one model over the other as the two models give very similar outcomes.

## 4 Predictive power of the models

This section is devoted to answer the following question: using only two MRI examinations given at time  $t_0$  and  $t_1$ , can we predict the volume and the shape of the tumor, at a later time  $t_2$ ? It is a very difficult question because – as seen in the last section – the patient variability cannot be perfectly explained using a model with less than two parameters. In particular, using only two time points, it is impossible to determine the behavior of the volume evolution, namely whether the volume evolution is linear, strictly convex or strictly concave. Indeed, determining  $\alpha$  (or  $\beta$ ),  $V_0$  and  $M_0$  using only the volumes at time  $t_0$  and  $t_1$  is an underdetermined problem. Using clinical characteristics (meningioma location, patient’s age and gender) and the times and volumes data, we have tried to classify the patients using machine learning techniques but found no interesting results.

### 4.1 Volume prediction

To answer this difficult question, we propose the following strategy. Let a patient denoted by  $p$  for which only two time data are available, we assume that a population of patients with at least 3 times is available and we will use this population to estimate the parameters of the patient  $p$  using the mixed-effect approach. We recall that the mixed-effect approach consists of pooling all the patients together and estimating a global distribution of the model parameters in the population. Our strategy can be seen as a way to compensate the lack

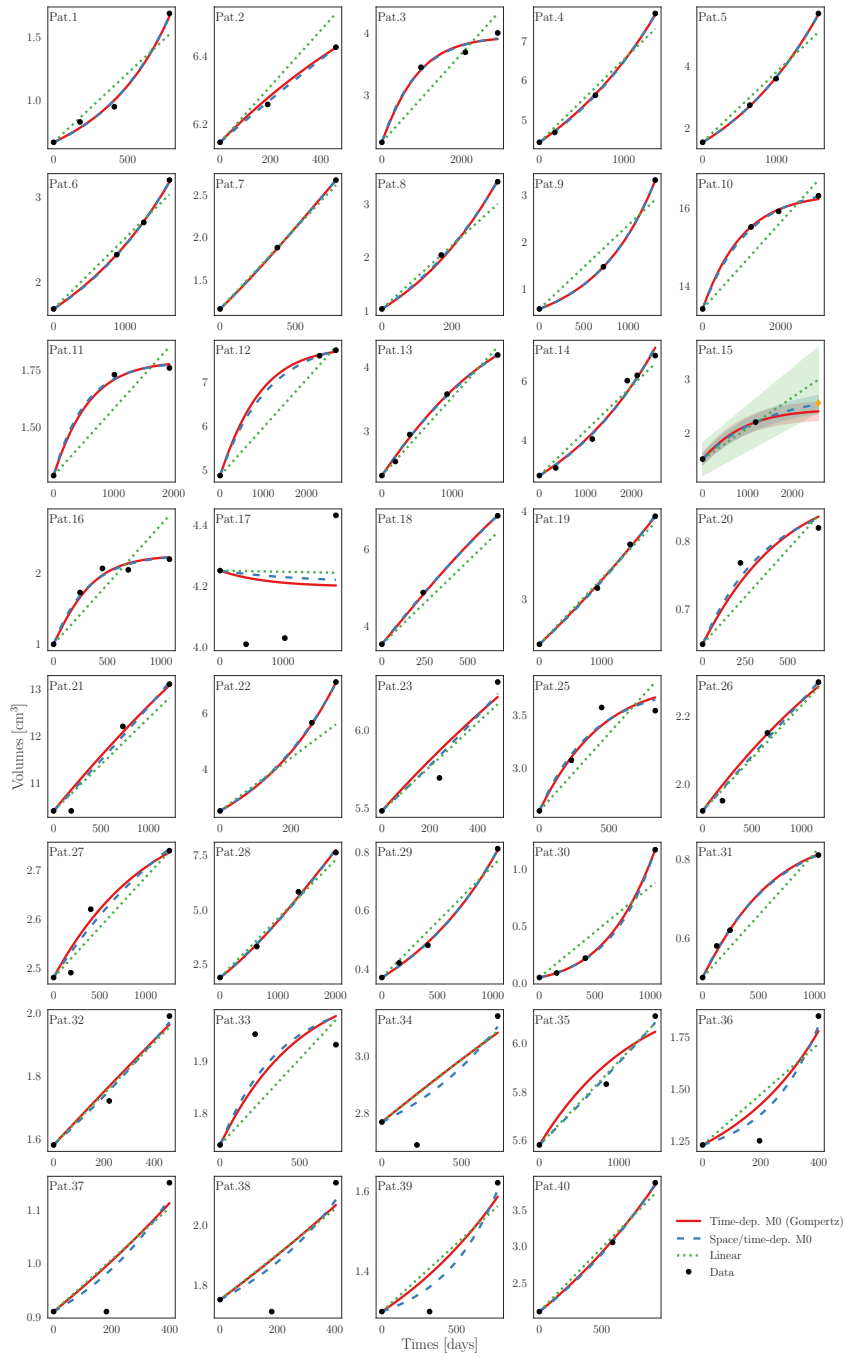


**Fig 3. Predictive power (see Patient 15) - Estimated volumes compared to the data for the full cohort. The tumor volumes obtained using MRI segmentations and used by the estimation process are represented by black circles. The orange diamond (see Patient 15) corresponds to the volume at time  $t_2$  which is not used to estimate the parameters. The red (resp. blue and green) curves correspond to the model with time-dependent growth rate (9) (resp. to the model with space- and time-dependent growth rate (10) and to the linear model (11)).**

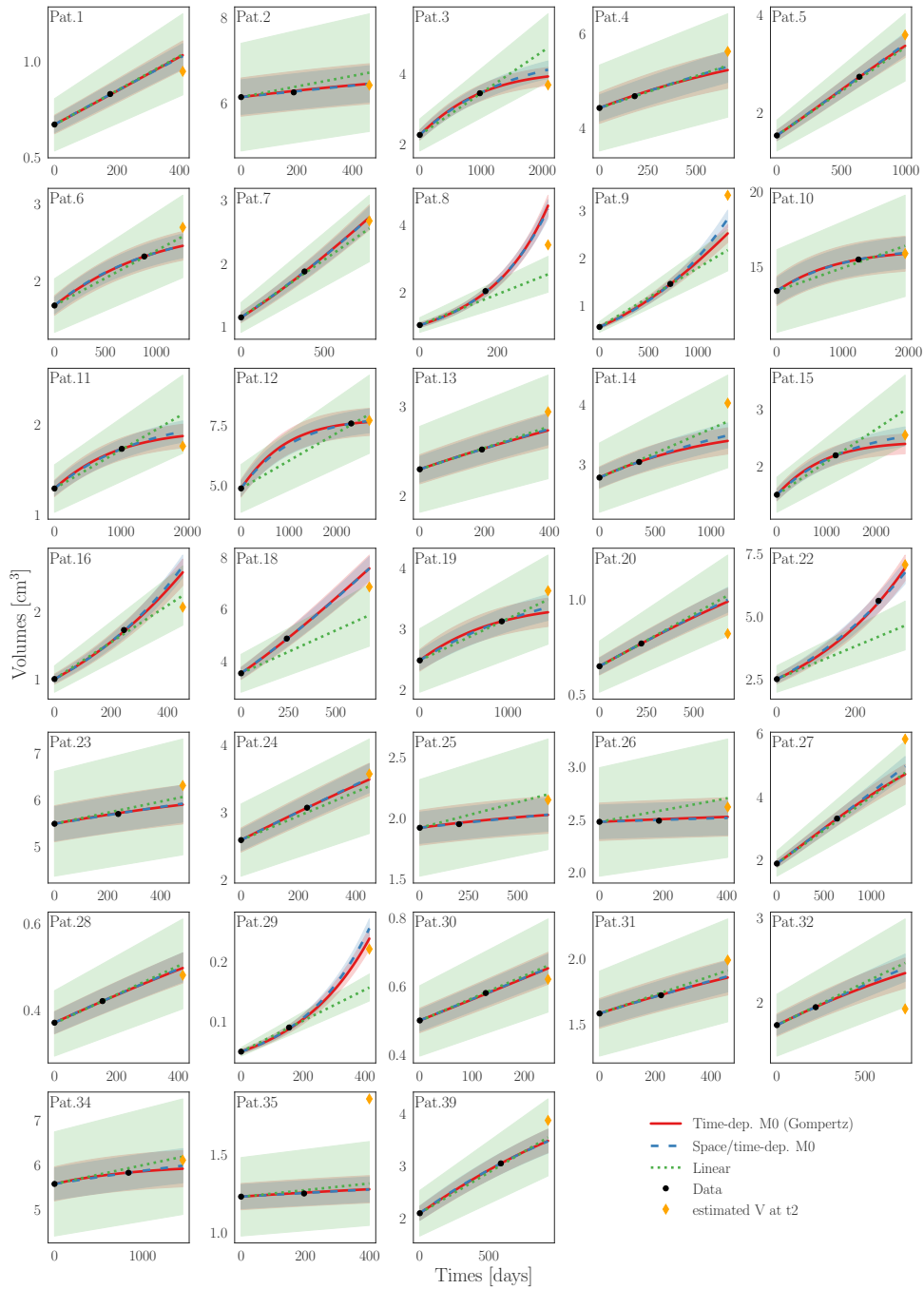


**Fig 4. Predictive power - Results obtained by applying the strategy presented in Section 4.1 to 33 patients. The tumor volumes obtained using MRI segmentations and used by the estimation process are represented by black circles. The orange diamond corresponds to the volume at time  $t_2$  which is not used to estimate the parameters. The red (resp. blue and green) curves correspond to the model with time-dependent growth rate (9) (resp. to the model with space- and time-dependent growth rate (10) and to the linear model (11)).**

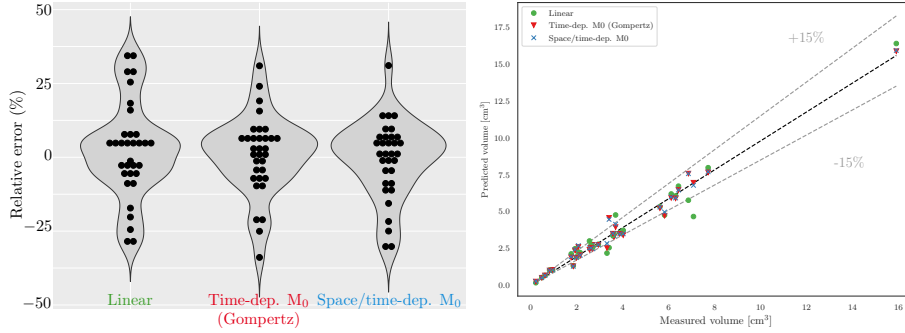


**Fig 5. Predictive power - Results obtained by applying the strategy presented in Section 4.1 to 33 patients. Left: Comparison of errors  $\mathcal{B}_p$ . Right: Comparison of the tumor volume predictions and measurements.**

of available times of the given patient  $p$  by an available population of  $N_p - 1$  patients. Fig 3 illustrates our strategy on Patient 15. All the time data of Patients from 1 to 14 and from 16 to 39 are used by the estimation process. Each figure gathers all the fits performed for each patient: the tumor volumes used for estimating the parameters are represented by black circles. The initial volume is not estimated in this strategy in order to increase the determination of the problem and to be compatible with 3D assessments. The red (resp. blue and green) curves correspond to the model with time-dependent growth rate (9) (resp. to the model with space- and time-dependent growth rate (10) and to the linear model (11)). The orange diamond (see figure of Patient 15) corresponds to the volume at time  $t_2$  which is not used to estimate the parameters. The strategy is applied for all the patients whose tumor volume at time  $t_1$  is strictly superior to the volume at time  $t_0$  (33 patients on 39), see Fig 4. Table 4 gives the error and the bias computed as

$$\mathcal{E}_p = 100 \frac{1}{N_p^s} \sum_{p=1}^{N_p^s} \frac{|V(t_2) - V_2^{meas}|}{V_2^{meas}} \text{ and } \mathcal{B}_p = \frac{1}{N_p^s} \sum_{p=1}^{N_p^s} \frac{V(t_2) - V_2^{meas}}{V_2^{meas}}, \quad (14)$$

where  $N_p^s$  corresponds to the number of patients whose the volume at time  $t_1$  is strictly superior to the volume at time  $t_0$  ( $N_p^s = 33$ ). The results are excellent. Using ODE systems, we can predict the volume at  $t_2$  with an error inferior to 10 % *i.e.* with the same order of magnitude of the segmentation error. Concerning the bias, it is smaller using ODE systems than linear model. Fig 5-left shows the relative error  $\frac{V(t_2) - V_2^{meas}}{V_2^{meas}}$  for each patient for the 3 models. In Fig 5-right, a comparison of the predicted volume with the measured volume at  $t_2$  has been done for the 33 patients. The grey lines permit the identification of outliers. One can remark that for some patients, the 3 models give similar results. For some other patients, the measured volume is included in the interval defined by the 3 predicted volumes. This motivates us to compare the mean of the predicted volumes to the measured volume: we obtain a global error of 9%. This strategy allows us to improve the volume prediction but cannot be used for the shape prediction.

Pat.	SDC (Time-d. $M_0$ )	SDC (Space/time-d. $M_0$ )	SDC (Redist.)
2	95%	95%	94%
4	93%	93%	93%
7	83%	83%	74%
8	87%	85%	69%
9	65%	63%	52%
11	85%	86%	82%
18	86%	86%	86%
20	90%	90%	87%
22	85%	84%	66%
23	87%	87%	88%

**Table 5. Predictive power - Sørensen-Dice coefficient SDC (see Eq. (13)) as a comparison between the solution of the tumor growth model and the MRI segmentation at the last available time.**

## 4.2 Shape prediction

Following the method presented in Section 3.2, we perform 3D simulations for 10 patients in order to assess the shape prediction of PDE models. We use the estimation process of parameters presented in the previous section. We compare the solutions of PDE models with the shape obtained by doing an expansion of the shape of the initial tumor using a redistancing process. To do that, we consider the level set of the initial shape with a volume equals to the volume predicted using the linear 0D model. Table 5 gives the Sørensen-Dice coefficient (SDC) measuring the similarity between simulations and registered MRI segmentations. Fig 6 presents 3D views of the solution of the model tumor growth with space- and time-dependent growth rate (red) compared to the MRI segmentation (blue) at the last available time. The supportive arachnoid tissue is represented by the white surface.

To conclude this section, one can see that the shape of the tumor is very well estimated with a mean of 85 % for PDE systems and 79 % for the linear model. The results are similar those obtained with the descriptive cases, which is very encouraging. On Fig 6, one can see as the shape of tumor of Patient 9 evolves in time, the difference between the predicted and the real shapes is important. The limitation of the linear model (which is not able to take into account the boundary of the skull) can be seen on the results of Patients 7, 8, 9 and 22. As previously, this section does not allow to select one PDE system. Both give similar results. This means that for meningioma, the hypothesis assuming that the growth rate is spatially independent seems realistic. This can be explained by the fact that the meningioma growth is slow.

## 5 Conclusion

In this work, we have introduced two PDE systems able to represent tumor growth. The growth rate is either assumed to be spatially dependent (*i.e.* decreases quicker inside the tumor) or assumed to be spatially independent (*i.e.* decreases at the same velocity inside or outside the tumor). The major advantage of these two models is that they depend only on two parameters and then can be adapted for each patient using observations that may be very sparse in time.

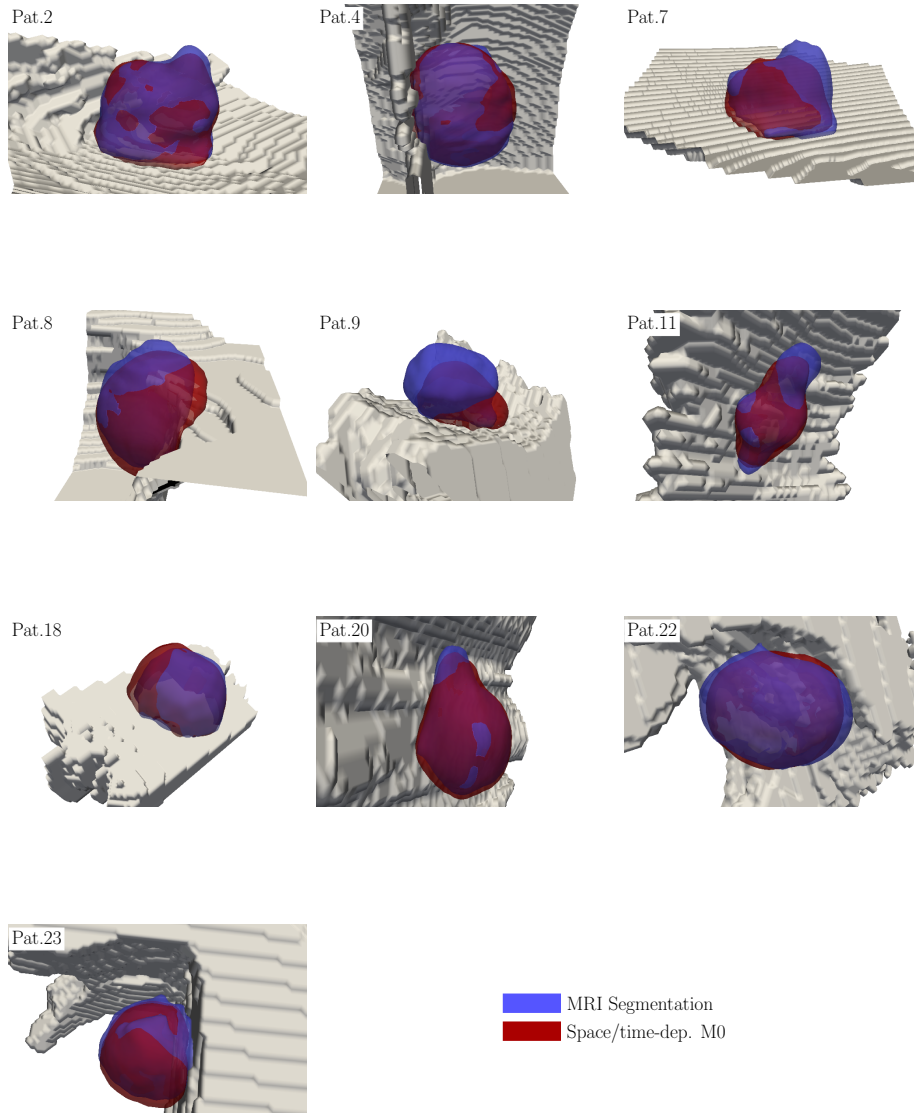


**Fig 6. Predictive power - 3D views of the solution of the model tumor growth with space- and time-dependent growth rate (red) compared to the MRI segmentation (blue) at the last available time for 10 patients. The supportive arachnoid tissue is represented by the white surface.**

After integration, these two models lead to two ODE systems that are used to estimate the parameters. In case of spatially-independent growth rate, the ODE system corresponds to the Gompertz model which is a very classical ODE model for tumor growth [36, 42–46].

The models have been retrospectively validated using a cohort of 39 patients with meningioma. This shows the descriptive power in terms of tumor volume and shape of our models. Then, we propose a strategy to predict the volume and the shape of the tumor at a later time using only two MRI examinations. Applying this strategy requires a population of patients with meningioma with at least three MRI examinations. Our results are very encouraging, provide a good insight on tumor growth and may help decide whether to extend the follow-up or to treat the tumor. Yet they have to be confirmed on a larger cohort. Work is also underway to consider additional covariates (*i.e.* clinical information of patients) to improve the accuracy of the prediction with machine learning to obtain a prior on meningioma behaviors. Three different patterns of growth are distinguishable in our cohort (linear, exponential or strictly concave.). These covariates may help determining the most likely pattern for a given patient and improve the personalization of the model by reducing the parameter search-space.

## Acknowledgments

This study was supported by the French Laboratory of Excellence TRAIL ANR-10-LABX-57. The authors would like to thank the POPRA program which is supported by the Conseil régional Nouvelle-Aquitaine and the European Funds FEDER.

## References

1. Swanson KR, Bridge C, Murray JD, Alvord Jr EC. Virtual and real brain tumors: using mathematical modeling to quantify glioma growth and invasion. *Journal of the neurological sciences*. 2003;216(1):1–10.
2. Colin T, Cornelis F, Jouganous J, Palussière J, Saut O. Patient-specific simulation of tumor growth, response to the treatment, and relapse of a lung metastasis: a clinical case. *Journal of Computational Surgery*. 2015;2(1):1.
3. Baratchart E, Benzekry S, Bikfalvi A, Colin T, Cooley LS, Pineau R, et al. Computational modelling of metastasis development in renal cell carcinoma. *PLoS computational biology*. 2015;11(11):e1004626.
4. Saut O, Lagaert JB, Colin T, Fathallah-Shaykh HM. A multilayer grow-or-go model for GBM: effects of invasive cells and anti-angiogenesis on growth. *Bulletin of mathematical biology*. 2014;76(9):2306–2333.
5. Benzekry S, André N, Benabdallah A, Ciccolini J, Faivre C, Hubert F, et al. Modeling the impact of anticancer agents on metastatic spreading. *Mathematical Modelling of Natural Phenomena*. 2012;7(1):306–336.

6. Ribba B, Kaloshi G, Peyre M, Ricard D, Calvez V, Tod M, et al. A tumor growth inhibition model for low-grade glioma treated with chemotherapy or radiotherapy. *Clinical Cancer Research*. 2012;18(18):5071–5080.
7. Ribba B, Saut O, Colin T, Bresch D, Grenier E, Boissel JP. A multi-scale mathematical model of avascular tumor growth to investigate the therapeutic benefit of anti-invasive agents. *Journal of theoretical biology*. 2006;243(4):532–541.
8. Baldi I, Gruber A, Alioum A, Berteaud E, Lebailly P, Huchet A, et al. Descriptive epidemiology of CNS tumors in France: results from the Gironde Registry for the period 2000–2007. *Neuro-oncology*. 2011;13(12):1370–1378.
9. Ostrom QT, Gittleman H, Farah P, Ondracek A, Chen Y, Wolinsky Y, et al. CBTRUS statistical report: Primary brain and central nervous system tumors diagnosed in the United States in 2006-2010. *Neuro-oncology*. 2013;15(suppl\_2):ii1–ii56.
10. Baldi I, Engelhardt J, Bonnet C, Bauchet L, Berteaud E, Grüber A, et al. Epidemiology of meningiomas. *Neurochirurgie*. 2018;64(1):5–14.
11. Hashiba T, Hashimoto N, Izumoto S, Suzuki T, Kagawa N, Maruno M, et al. Serial volumetric assessment of the natural history and growth pattern of incidentally discovered meningiomas. *Journal of neurosurgery*. 2009;110(4):675–684.
12. Nakasu S, Fukami T, Nakajima M, Watanabe K, Ichikawa M, Matsuda M. Growth pattern changes of meningiomas: long-term analysis. *Neurosurgery*. 2005;56(5):946–955.
13. Johnson DR, Olson JE, Vierkant RA, Hammack JE, Wang AH, Folsom AR, et al. Risk factors for meningioma in postmenopausal women: results from the Iowa Women’s Health Study. *Neuro-oncology*. 2011;13(9):1011–1019.
14. Krampla W, Newrkla S, Pfisterer W, Jungwirth S, Fischer P, Leitha T, et al. Frequency and risk factors for meningioma in clinically healthy 75-year-old patients: Results of the Transdanube Ageing Study (VITA). *Cancer: Interdisciplinary International Journal of the American Cancer Society*. 2004;100(6):1208–1212.
15. Vernooij MW, Ikram MA, Tanghe HL, Vincent AJ, Hofman A, Krestin GP, et al. Incidental findings on brain MRI in the general population. *New England Journal of Medicine*. 2007;357(18):1821–1828.
16. Braunstein JB, Vick NA. Meningiomas: the decision not to operate. *Neurology*. 1997;48(5):1459–1462.
17. Gupta A, Xu Z, Cohen-Inbar O, Snyder MH, Hobbs LK, Li C, et al. Treatment of asymptomatic meningioma with gamma knife radiosurgery: Long-term follow-up with volumetric assessment and clinical outcome. *Neurosurgery*. 2019;.

18. Islim AI, Mohan M, Moon RD, Srikandarajah N, Mills SJ, Brodbelt AR, et al. Correction to: Incidental intracranial meningiomas: a systematic review and meta-analysis of prognostic factors and outcomes. *Journal of neuro-oncology*. 2019;144(2):427–429.
19. Kim KH, Kang SJ, Choi JW, Kong DS, Seol HJ, Nam DH, et al. Clinical and radiological outcomes of proactive Gamma Knife surgery for asymptomatic meningiomas compared with the natural course without intervention. *Journal of neurosurgery*. 2018;130(5):1740–1749.
20. Mohammad MH, Chavredakis E, Zakaria R, Brodbelt A, Jenkinson MD. A national survey of the management of patients with incidental meningioma in the United Kingdom. *British journal of neurosurgery*. 2017;31(4):459–463.
21. Romani R, Ryan G, Benner C, Pollock J. Non-operative meningiomas: long-term follow-up of 136 patients. *Acta neurochirurgica*. 2018;160(8):1547–1553.
22. Zeng L, Liang P, Jiao J, Chen J, Lei T. Will an asymptomatic meningioma grow or not grow? A meta-analysis. *Journal of Neurological Surgery Part A: Central European Neurosurgery*. 2015;76(05):341–347.
23. Couldwell WT. Asymptomatic meningiomas. *Journal of neurosurgery*. 2006;105(4):536–537.
24. Islim AI, Mohan M, Moon RD, Srikandarajah N, Mills SJ, Brodbelt AR, et al. Incidental intracranial meningiomas: a systematic review and meta-analysis of prognostic factors and outcomes. *Journal of neuro-oncology*. 2019;142(2):211–221.
25. Jo KW, Kim CH, Kong DS, Seol HJ, Nam DH, Park K, et al. Treatment modalities and outcomes for asymptomatic meningiomas. *Acta neurochirurgica*. 2011;153(1):62–67.
26. Nakamura M, Roser F, Michel J, Jacobs C, Samii M. The natural history of incidental meningiomas. *Neurosurgery*. 2003;53(1):62–71.
27. Nakasu S, Nakasu Y, Fukami T, Jito J, Nozaki K. Growth curve analysis of asymptomatic and symptomatic meningiomas. *Journal of neuro-oncology*. 2011;102(2):303–310.
28. Oya S, Kim SH, Sade B, Lee JH. The natural history of intracranial meningiomas. *Journal of neurosurgery*. 2011;114(5):1250–1256.
29. Sughrue ME, Rutkowski MJ, Aranda D, Barani IJ, McDermott MW, Parsa AT. Treatment decision making based on the published natural history and growth rate of small meningiomas: a review and meta-analysis. *Journal of neurosurgery*. 2010;113(5):1036–1042.
30. Zeidman LA, Ankenbrandt WJ, Du H, Paleologos N, Vick NA. Growth rate of non-operated meningiomas. *Journal of neurology*. 2008;255(6):891–895.

31. Layne KA, Dargan PI, Archer JR, Wood DM. Gadolinium deposition and the potential for toxicological sequelae—A literature review of issues surrounding gadolinium-based contrast agents. *British journal of clinical pharmacology*. 2018;84(11):2522–2534.
32. Brugada-Bellsolà F, Rodríguez PT, Rodríguez-Hernández A, Garcia-Armengol R, Tardáguila M, González-Crespo A, et al. Growth prediction in asymptomatic meningiomas: the utility of the AIMSS score. *Acta Neurochirurgica*. 2019;161(11):2233–2240. doi:10.1007/s00701-019-04056-3.
33. Lee EJ, Kim JH, Park ES, Kim YH, Lee JK, Hong SH, et al. A novel weighted scoring system for estimating the risk of rapid growth in untreated intracranial meningiomas. *Journal of neurosurgery*. 2017;127(5):971–980.
34. Lee EJ, Park JH, Park ES, Kim JH. Wait-and-see strategies for newly diagnosed intracranial meningiomas based on the risk of future observation failure. *World neurosurgery*. 2017;107:604–611. doi:10.1016/j.wneu.2017.08.060.
35. Lachaud JO, Taton B. Deformable model with a complexity independent from image resolution. *Computer Vision and Image Understanding*. 2005;99(3):453–475.
36. Benzekry S, Lamont C, Beheshti A, Tracz A, Ebos JM, Hlatky L, et al. Classical mathematical models for description and prediction of experimental tumor growth. *PLoS computational biology*. 2014;10(8):e1003800.
37. Ribba B, Holford NH, Magni P, Trocóniz I, Gueorguieva I, Girard P, et al. A review of mixed-effects models of tumor growth and effects of anticancer drug treatment used in population analysis. *CPT: pharmacometrics & systems pharmacology*. 2014;3(5):1–10.
38. Cornelis F, Martin M, Saut O, Buy X, Kind M, Palussiere J, et al. Precision of manual two-dimensional segmentations of lung and liver metastases and its impact on tumour response assessment using RECIST 1.1. *European radiology experimental*. 2017;1(1):16.
39. Antony, France: Lixoft SAS. Monolix version 2019R1; 2019. Available from: <http://lixoft.com/products/monolix/>.
40. Kuhn E, Lavielle M. Maximum likelihood estimation in nonlinear mixed effects models. *Computational Statistics & Data Analysis*. 2005;49(4):1020–1038.
41. Kritter T. Utilisation de données cliniques pour la construction de modèles en oncologie. Bordeaux; 2018.
42. Casey AE. The experimental alteration of malignancy with an homologous mammalian tumor material: I. Results with intratesticular inoculation. *The American Journal of Cancer*. 1934;21(4):760–775.
43. Gompertz B. XXIV. On the nature of the function expressive of the law of human mortality, and on a new mode of determining the value of life contingencies. In a letter to Francis Baily, Esq. FRS &c. *Philosophical transactions of the Royal Society of London*. 1825;(115):513–583.

44. Laird AK. Dynamics of tumour growth. British journal of cancer. 1964;18(3):490.
45. Laird AK. Dynamics of tumour growth: comparison of growth rates and extrapolation of growth curve to one cell. British Journal of Cancer. 1965;19(2):278.
46. Norton L. A Gompertzian model of human breast cancer growth. Cancer research. 1988;48(24 Part 1):7067–7071.

## Appendix

In order to prove Propositions 1 and 2, we will prove the following lemma.

**Lemma 1** *Let  $\bar{M}(t)$  the mean carrying capacity*

$$\bar{M}(t) = \int_{\Omega(t)} M(t, X) dX,$$

*the quantity  $V(t)$  satisfies the following ODE:*

$$V'(t) = \bar{M}(t).$$

**Proof** Let us compute  $V'(t)$ . Using Reynold's theorem and Eq (1), we get

$$V'(t) = \frac{d}{dt} \int_{\Omega(t)} dX = \int_{\partial\Omega(t)} (\vec{v} \cdot \vec{n}) d\sigma,$$

where  $\vec{n}$  is the outward normal to  $\partial\Omega(t)$ . Green theorem shows that  $\int_{\partial\Omega} \vec{v} \cdot \vec{n} d\sigma = \int_{\Omega(t)} \nabla \cdot \vec{v} dX$ . Thanks to Eq (3), it follows that

$$V'(t) = \frac{d}{dt} \int_{\Omega(t)} dX = \int_{\Omega(t)} MT dX = \int_{\Omega(t)} M dX,$$

since  $T$  is identically equal to 1 inside  $\Omega(t)$ . This last identity leads to

$$V'(t) = \bar{M}(t). \tag{15}$$

□

**Proof** (Proposition 1) We can compute  $\bar{M}(t)$

$$\bar{M}(t) = \int_{\Omega(t)} M(t) dX = \int_{\Omega(t)} M_0 e^{-\alpha t} dX = M_0 e^{-\alpha t} V(t).$$

This implies that

$$V'(t) = M_0 e^{-\alpha t} V(t).$$

This is easily solved and one gets

$$V(t) = V_0 e^{\frac{M_0}{\alpha}(1-e^{-\alpha t})}.$$

One can recognize the formula of the Gompertz model, a very classical growth model, see [36] for a full study and [42–46] for validations of Gompertz model for tumor growth. □

**Proof** (Proposition 2) We can compute  $\bar{M}'(t)$  using Reynold's theorem:

$$\begin{aligned}\bar{M}'(t) &= \frac{d}{dt} \int_{\Omega(t)} M(t, X) dX = \int_{\Omega(t)} \partial_t M dX + \int_{\partial\Omega(t)} (\vec{v} \cdot \vec{n}) M d\sigma \\ &= - \int_{\Omega(t)} \alpha M T dX + \int_{\partial\Omega(t)} (\vec{v} \cdot \vec{n}) M d\sigma.\end{aligned}$$

Now, recall that  $T$  is identically equal to 1 within the tumor  $\Omega(t)$  and  $M$  is identically equal to  $M_0$  on the boundary  $\partial\Omega(t)$ . Therefore

$$\bar{M}'(t) = -\alpha \int_{\Omega(t)} M dX + M_0 \int_{\partial\Omega} (\vec{v} \cdot \vec{n}) d\sigma.$$

As previously, using Green formula and Eq (3), we have

$$\begin{aligned}\bar{M}'(t) &= -\alpha \int_{\Omega(t)} M dX + M_0 \int_{\Omega(t)} M T dX \\ &= (M_0 - \alpha) \int_{\Omega(t)} M dX = (M_0 - \alpha) \bar{M}.\end{aligned}$$

It follows

$$\bar{M}'(t) = (M_0 - \alpha) \bar{M}(t). \quad (16)$$

System Eq (15)-(16) can be solved and one gets

$$\bar{M}(t) = \bar{M}_0 e^{(M_0 - \alpha)t} = M_0 V_0 e^{(M_0 - \alpha)t},$$

and  $V'(t) = M_0 V_0 e^{(M_0 - \alpha)t}$  leads to

$$V(t) = V_0 + M_0 V_0 \frac{e^{(M_0 - \alpha)t} - 1}{M_0 - \alpha}.$$

□